

# Flow Characterization of the ADVANTAGE<sup>®</sup> and St. Jude Medical<sup>®</sup> Bileaflet Mechanical Heart Valves

Mark C. S. Shu, Keith K. O'Rourke<sup>1</sup>, Chris M. Coppin, Jack D. Lemmon

Medtronic Heart Valves, Inc., Santa Ana, CA, <sup>1</sup>Adaptive Research Inc., Alhambra, CA, USA

**Background and aim of the study:** The study aim was to characterize time-dependent flow fields and flow structures within the ADVANTAGE<sup>®</sup> (ADV) and St. Jude Medical<sup>®</sup> (SJM) prosthetic bileaflet mechanical heart valves.

**Methods:** Three-dimensional unsteady computational fluid dynamic simulations were conducted in the aortic position for both valves. Flow boundary conditions were acquired from an in-vitro experiment. The governing equations were solved by a finite volume method that employed a moving cell technique to simulate the motion of the valve leaflet in the cardiac cycle. The computed velocities were subsequently validated using the velocities measured in the in-vitro experiment.

**Results:** Both valves had similar flow phenomena at the geometric symmetry plane of the valve housing, and both experienced a waterhammer effect upon

closure. However, flow characteristics in the pivots differed distinctively between both valves. More dynamic flow activity was observed at the bi-level butterfly pivots of the ADV valve. Flow vena contracta and large flow boundary separation zones at the central flow orifice were captured adjacent to the pivots of the SJM valve. During valve opening, retrograde systolic flow at the bottom of the pivot was observed. No persistent flow stases were seen in the pivots of either valves.

**Conclusion:** Although overall flow characterization for both valves was similar, flow features within each valve's pivots correlated to the pivot design. The bi-level butterfly pivot design of the ADV valve appeared to provide relatively easy passages for pivot flow washing.

The Journal of Heart Valve Disease 2004;13:814-822

Bileaflet mechanical heart valves (BMHVs) have been widely used to replace diseased natural heart valves in surgical treatment since the introduction of the St. Jude Medical valve in 1977. Although the design of mechanical heart valves is structurally robust, the mitigation of thrombogenic flow conditions in a valve design remains a challenge (1-9).

A BMHV typically consists of a rigid, annular valve housing and a pair of rotatable leaflets. Each leaflet is retained inside the valve housing by a pair of small pivots. These pivots control the range of leaflet motion as the leaflets rotate passively, responding to blood flow pressure gradients.

Each valve design produces unique flow fields within and distal to the valve housing. Distal flow structures from various mechanical prostheses have been

studied in vitro, both qualitatively and quantitatively, for over two decades (10-15). Although some studies have obtained laser Doppler velocimetry data with coarse grids within the pivots (4,5), detailed flow features within the valve housing and the valve pivots are impractical to acquire in this manner due to experimental limitations, the complex structures of BMHVs, and the movement of the leaflets.

To compensate for experimental limitations, both steady and unsteady computational fluid dynamic (CFD) simulations have been widely used to replicate flow fields proximal and distal to a prosthetic mechanical heart valve (16-20). The first unsteady three-dimensional (3-D) CFD simulation to reveal flow fields within the pivot of a BMHV was reported in 1996 (3). This simulation used a two-tier process that separately calculated the flow domains in the valve housing and in the valve pivot, and then combined the results for analysis. Results from this study revealed that persistent flow stases within the valve pivots might be the essential cause of thrombus formation. Similar steady-state or time-dependent CFD simulations have since

---

Address for correspondence:  
Mark C. S. Shu PhD, Medtronic Heart Valves, 1851 East Deere Ave.,  
Santa Ana, CA 92705, USA  
e-mail: shum1@medtronic.com

been used to evaluate flow phenomena within valve pivots for other BMHV designs (21-23). However, the accuracy of these simulations was insufficient because they lacked either dynamic characteristics or experimental flow boundary conditions and experimental validation.

The present study employed a single-step computational simulation method to characterize flow through the Medtronic ADVANTAGE<sup>®</sup> (ADV) and the St. Jude Medical<sup>®</sup> (SJM) bileaflet mechanical valves. The CFD models were created as per the dimensions of the aortic segments in an in-vitro experiment. The simulations were carried out using the flow boundary conditions acquired from the experiment, and the simulation results were validated by the experiment. The flow fields and flow features of both valves were compared in detail at the geometric symmetry plane of the valves and within the pivots.

## Materials and methods

The basic design features of the ADV and SJM valves are presented in Figure 1, and have been reported earlier (24). Each valve has a housing and two leaflets. For the ADV valve, each leaflet is constrained and retained within the valve housing by a pair of bi-level butterfly pivots. Each bi-level butterfly pivot consists of a primary flat, a butterfly recess, and a secondary flat (Fig. 1, upper). In comparison to the primary flat, the secondary flat is recessed into the valve housing by approximately one-third of the depth of the pivot recess. Profiling the secondary flat lower than the primary flat level creates a flow channel over the secondary flat. By comparison, each SJM valve's leaflet is retained by one pair of single level butterfly pivots constructed on pivot guards extending from the valve housing (Fig. 1, lower). The central flow orifice between the open leaflets comprises 22% of the flow area in the ADV valve compared to 18% in the SJM valve. The open to closed leaflet angles for the ADV and SJM valves are 86° to 22° and 85° to 25°, respectively (Fig. 1).

The CFD simulations in the present study were conducted at the aortic position. The 3-D CFD models were constructed as per the dimensions in a pulse duplicator (Fig. 2). The aortic sinus was assumed to be an axisymmetric structure. The ADV valve in the CFD model was constructed as per the manufacturer's computer-aided design (CAD) dimensions for a 29 mm ADV valve, while the SJM valve in its CFD model was created as per the dimensions of a clinical quality 29 mm valve as measured with a coordinate-measuring machine at an accuracy of 0.001". Taking advantage of the geometric symmetry of a BMHV, the simulation used only one-quarter of the valve housing, and one-half of one leaflet.

The flow domain of each CFD model consisted of flow in the valve housing and flow through the valve pivots. The flow domain was divided into a number of cells, with each cell being constructed using transfinite interpolation. Approximately 40,000 cells were generated for each model using a variable cell mesh. A coarse cell mesh was used proximal from and distal to the valve housing, whereas a fine cell mesh was used inside the housing and pivot. To simulate leaflet motion throughout a cardiac cycle, this simulation incorporated a moving cell (3-D volume grid) technique.

The governing equations used in this CFD simulation were mass conservation and time-dependent Navier-Stokes equations:

$$\frac{\partial \rho}{\partial t} + \frac{\partial}{\partial x_j} (\rho u_j) = 0, \quad (1)$$

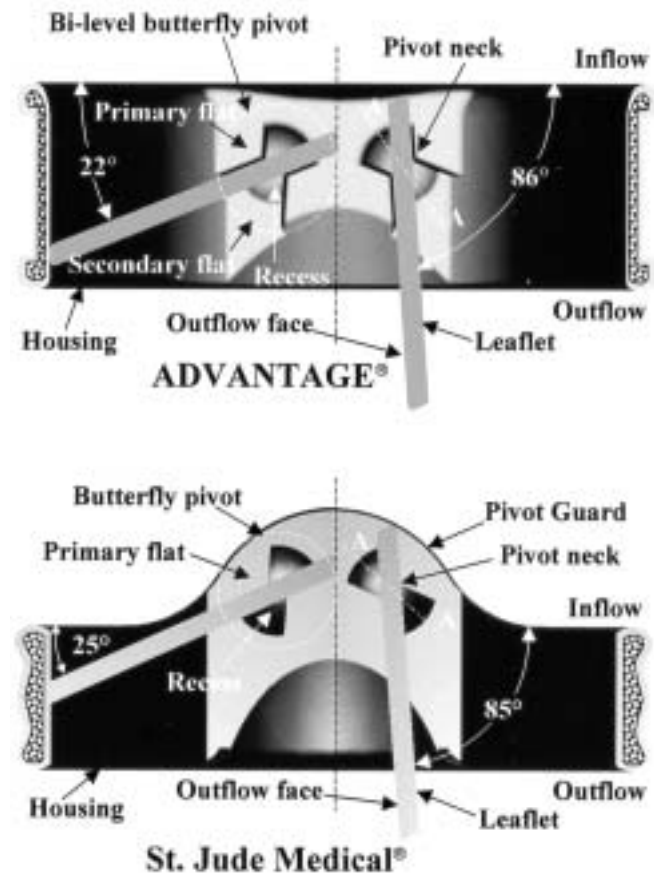


Figure 1: Each diagram shows half of a valve cut along the valve's geometric symmetry plane. The ADVANTAGE valve's bi-level butterfly pivot consists of a primary flat, a recess and a secondary flat recessed from the primary flat. The pivot is bi-level about the pivot neck. The St. Jude Medical valve's single level butterfly pivot includes a primary flat and a recess. The pivots are created on the pivot guard extending from the valve housing. The section A-A is perpendicular to the recess.

$$\frac{\partial u_i}{\partial t} + u_j \frac{\partial u_i}{\partial x_j} = -\frac{1}{\rho} \frac{\partial p}{\partial x_i} + \frac{\mu}{\rho} \frac{\partial^2 u_i}{\partial x_j \partial x_j} + X_i. \quad (2)$$

where the density,  $\rho$ , was a constant for incompressible fluid,  $u$  was the velocity,  $\mu/\rho$  was the kinematic viscosity of the fluid, and  $X_i$  was the body force per unit volume. These equations were solved using a finite volume method with a pressure-based algorithm for continuity, and a Pressure-Implicit with Splitting of Operators algorithm for pressure-velocity coupling (25). The solution scheme was based on a strongly conservative formulation for the Navier-Stokes equations, and the turbulent  $k-\epsilon$  model was incorporated. The numerical method for solving Equations (1) and (2) consisted of the discretization of the equations on a computational grid, the formation of a set of algebraic equations, and solution of the algebraic equations. The numerical method yielded a discrete solution of the flow domain, which was comprised of the values of the flow variables at the grid points.

The simulations were conducted using a commercial CFD program (CFD2000 STORM; Adaptive-Research, Alhambra, CA, USA). To eliminate potential acceleration errors imposed on the pressure and flow fields at the beginning of the valve opening, two computation runs were employed in the simulation. For the first run, the initial velocities and pressures inside the flow domains were set at zero, and the governing equations were solved in a cardiac cycle. The final velocity and pressure distributions inside the flow domains from the first run were then used as the initial velocities and pressures for the second run. The results reported were derived from the second run.

The flow boundary conditions for the CFD simulations were obtained experimentally from pulse duplication (24). The pulse duplication conditions included a cardiac rhythm of 70 beats/min, a cardiac output of 5 l/min, and aortic pressures of 120/80 mmHg. Each resulting aortic mass flux as a function of time was applied uniformly to the inlet surface of the corresponding CFD model. The boundary velocity calculated from the mass flux was directed into the domain normal to the cell surface. The flow pressure was fixed at zero at the outlet surface because only the pressure gradient was relevant and required for the CFD simulation. Symmetric boundary flow conditions were applied on the planes of symmetry along the axial direction; at each symmetry plane, the velocity normal to the boundary was set to zero and for all variables the gradient normal to the boundary was also set to zero. The solid surfaces of the flow domain were treated as impermeable boundaries. To simulate valve leaflet motion, the measured leaflet movement was supplied as a prescribed leaflet movement boundary

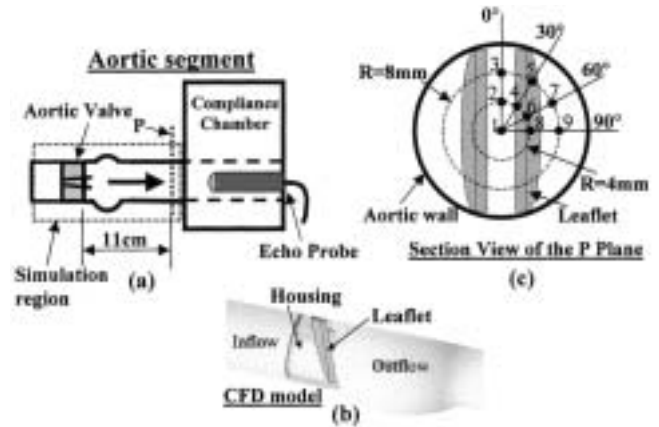


Figure 2: The CFD model duplicated the dimensions of the simulation region in the aortic segment (a) of a pulse duplicator. The valve portion of the CFD model is shown in (b). In (a), the plane P is the interrogation plane. The echo Doppler velocities were measured at nine locations in one quadrant of the plane, as shown in (c).

condition. In the in-vitro experiments, the leaflet motion in a cardiac cycle was measured using a Kodak EktaPro Motion Analyzer (Model 2000; Eastman Kodak Co., San Diego, CA, USA) set at 1,000 frames per second.

The CFD simulation was validated by comparing the calculated flow velocities at nine locations with measured echo Doppler velocities at the same locations. The echo Doppler velocities were measured in the aortic segment of the pulse duplicator using an echo Doppler system (HP Sonos 1000CF; Hewlett-Packard Company, Andover, MA, USA). The nine measurement locations were defined on an interrogation plane (Fig. 2). This plane was distal from the aortic valve by 11 cm (more than three diameters of the aorta) to ensure that the measurement was conducted in a region with fully developed flow velocity. Because of the geometric symmetry of a BMHV, the Doppler velocities were acquired in only one quadrant of the aorta.

The simulation results were reported in a temporal sequence at opening (28 ms), peak systole (72 ms), closing (300 ms) and closed (520 ms) during the cardiac cycle. The results were presented on the geometric symmetry plane defined in Figure 1, on the planes A through D at the pivot (Fig. 3), and on the plane created by the A-A section view (Fig. 1). For the ADV valve, Plane C in Figure 3 penetrated into the primary flat and was slightly away from the secondary flat, and Plane D in Figure 3 penetrated into both the primary and secondary flats. For the SJM valve, both Planes C and D penetrated into its primary flat.

## Results

The comparison at the nine locations between the calculated velocity profiles and the measured echo Doppler velocity profiles demonstrated a close agreement in both magnitudes and profile contours. The comparison results (Fig. 4) were acquired along locations 1 to 3 on the interrogation plane, as defined in Figure 2. For the ADV valve, the computed and the measured velocity profiles closely resembled each other in a cardiac cycle. For the SJM valve, the computed and the measured velocity profiles also closely matched each other. This agreement validated the CFD simulations for both valves.

The CFD simulation results are presented in Figures 5, 6, 7, 8, and 9. Mirror images of the calculated results from the quarter-valve were used to present a full image of the valve. The length and direction of each velocity vector designated the magnitude and direction of flow, respectively. The colors on each color bar represented the flow pressure.

Similar flow characteristics were revealed from the CFD results on the geometric symmetry plane of both valves (Fig. 5). As the leaflets opened under a positive pressure gradient, a jet flow was seen through the central flow orifice between the leaflets. As shown in diagrams (c) and (d), the intensity and width of this jet increased as left ventricular pressure rose and the leaflets opened further. For the SJM valve, the denser and larger velocity vectors indicated a stronger central

jet at peak systole. The flow boundary separation zone adjacent to the leaflet outflow face was more evident for the SJM valve because of the stronger central jet. For both valves, large vortices developed inside the sinuses of Valsalva (SV).

When the pressure gradient was reversed, the leaflets were driven to close and vortices inside the SV were diminished (see Fig. 5e and f). Upon valve closure, the pressure distribution on the inflow and outflow faces of the leaflets revealed that negative pressures were generated at the leaflet's inflow face, and positive pressures built up on the leaflet's outflow face. The lowest pressure (dark blue), which could approach the magnitude of negative 200 mmHg for both valves, occurred near the leaflet tip on the inflow side. This phenomenon was attributed to the water-

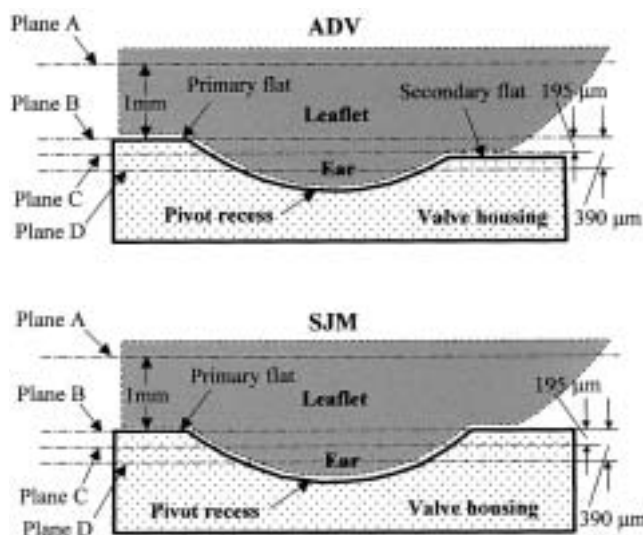


Figure 3: Schematic diagram showing the A-A section view in Figure 1. The CFD results are presented on Plane A (1 mm away from the primary flat) and within the pivots (Planes B to D). Plane B is level with the primary flat.

Plane C penetrates only one side of the ADV valve housing, and both sides of the SJM valve housing. Plane D is inside the pivot recess.

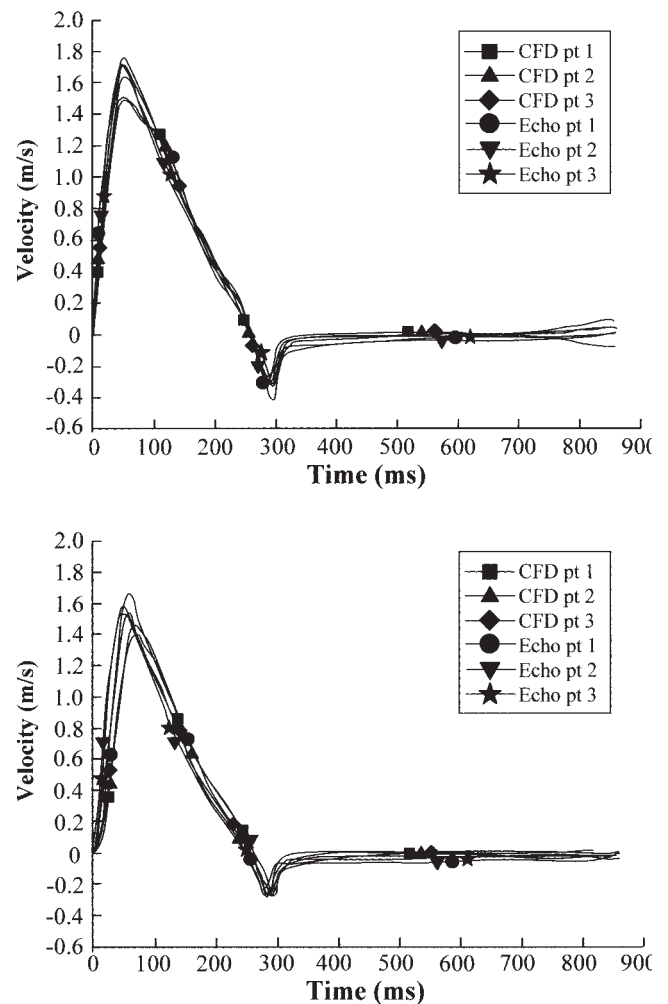


Figure 4: Velocity comparison between the calculated velocities and the echo Doppler velocities at locations 1 to 3, as defined in Figure 2. The comparison shows that the magnitudes and profile contours of the computed velocities closely match those of the Doppler velocities for both valves.

hammer effect upon valve closure, and occurred only for a short time (less than 200  $\mu$ s) in the CFD simulation. After the valve was fully closed, no flow was seen through the leaflets and velocity vectors in the flow domains diminished to zero (not shown).

Distinctly different flow characteristics between the ADV and SJM valves were demonstrated adjacent to/within the pivots by the CFD results (Figs. 6 and 7). The results were shown at planes A, B, and C, as defined in Figure 3. At peak systole, the CFD results at Plane A showed that the vena contracta in the central flow orifice of the SJM valve was more pronounced than that of the ADV valve. Large flow boundary separation zones could be observed adjacent to the outflow faces of the SJM leaflets. Flow through the SJM valve converged toward the center of the SV. At Planes B and C, velocity vectors indicated flow through the channel created by the secondary flat of the ADV. Because Plane B was level with the primary flat, no flow was seen in the central flow orifice. Although

Plane C was at one-third of the depth of the pivot recess, the ADV valve's secondary flat could still be seen to provide an easy passage for flow through the pivot recess as indicated by the velocity vectors (Fig. 6). For the SJM valve, velocity vectors were confined in the recess by the recess geometry. When the leaflets were closing (Fig. 7), they wiped through the pivots, and the vena contracta in the central flow orifice was replaced by reversing flow on Plane A. On Planes B and C, velocity vectors showed reversing flow through the channel created by the secondary flat of the ADV.

Similar flow phenomena were seen on Plane D for both valves (Fig. 8). Because Plane D was at two-thirds of the depth of the pivot recess, flow in this plane was bounded by the recess walls. As the leaflet ear wiped through the pivot during opening, the velocity vectors

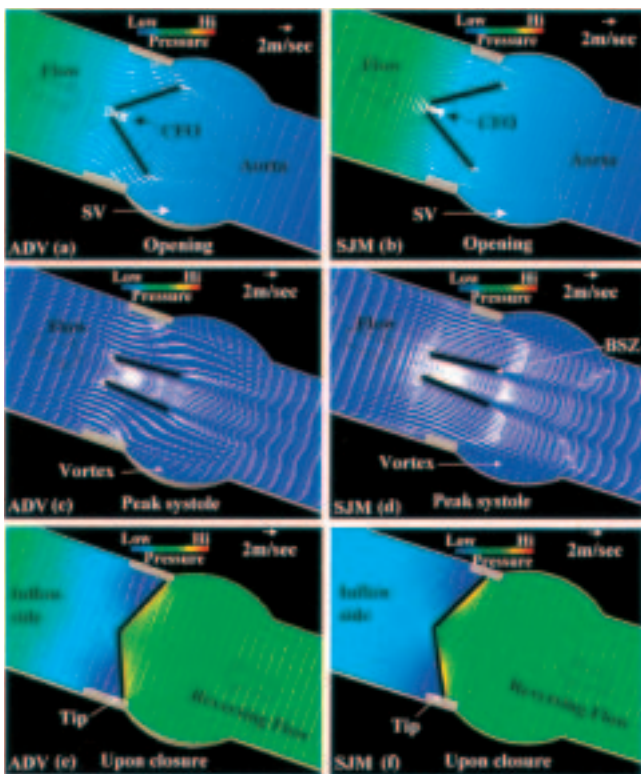


Figure 5: CFD results show similar flow features for both valves on the geometric symmetry plane. A jet flow occurs at the central flow office (CFO). At peak systole, a boundary separation zone (BSZ) near the leaflet outflow face is more evident in the SJM valve than in the ADV valve. Vortices form inside the sinuses of Valsalva (SV) for both valves. Upon valve closure, a waterhammer effect is observed, with pressure building up on the leaflet outflow faces and pressure falling at the inflow faces near the leaflet tips.

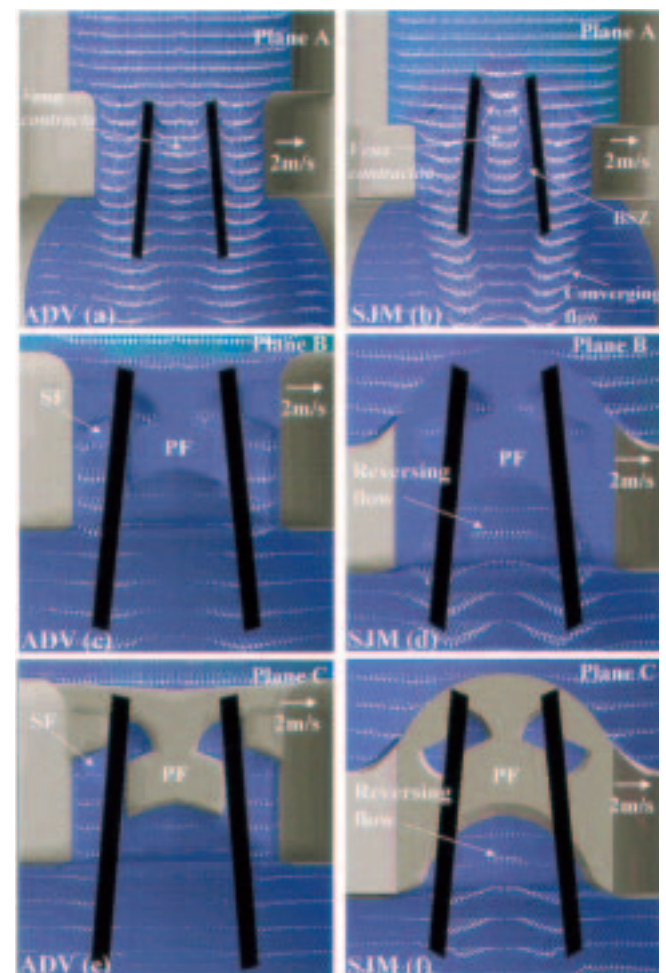


Figure 6: At peak systole, the CFD results on Plane A show that the SJM has a stronger vena contracta, converged flow with higher velocities, and a clearly delineated boundary separation zone (BSZ). On Planes B and C, flow can be seen along the channel created by the ADV valve's secondary flat (SF), while reversing flow occurs distal from the SJM valve's primary flat (PF).

seen within the pivot recess of the ADV valve were larger than those observed within the SJM valve. The velocities reached 0.3 m/s for the ADV valve and 0.20 m/s for the SJM. This indicated a more dynamic flow with better flow washing within the ADV pivot recess than within the SJM pivot recess. Velocity vectors at peak systole demonstrated a reversal of flow within the recesses of both valves. After closure, flow leakage through the recesses could be observed for both valves. The CFD results at Plane D also showed no persistent flow stagnation regions within the recesses of either valves.

For both pivot designs, the leaflet ear closely matches the contour of the pivot recess with a small gap at the bottom of the recess. On the plane created by the A-A section view in Figure 1, the CFD results revealed the gap flow between the leaflet ear and the bottom of

the recess (Fig. 9). Forward flow and leakages were seen within the gaps of both valves. At peak systole, retrograde gap flow was seen in both valves. The results indicated that with larger velocity vectors, the ADV valve had a relatively stronger gap flow at the bottom of the pivot recess than the SJM valve.

## Discussion

The present study reveals the flow characteristics of the ADV and SJM valves using 3-D time-dependent CFD simulations. These simulations utilized the realistic dimensions of the ADV and SJM valves in conjunction with in-vitro experimental data to construct 3-D flow models. The results of the simulations were compared to results acquired from the in-vitro pulse duplicator from which the CFD input flow boundary

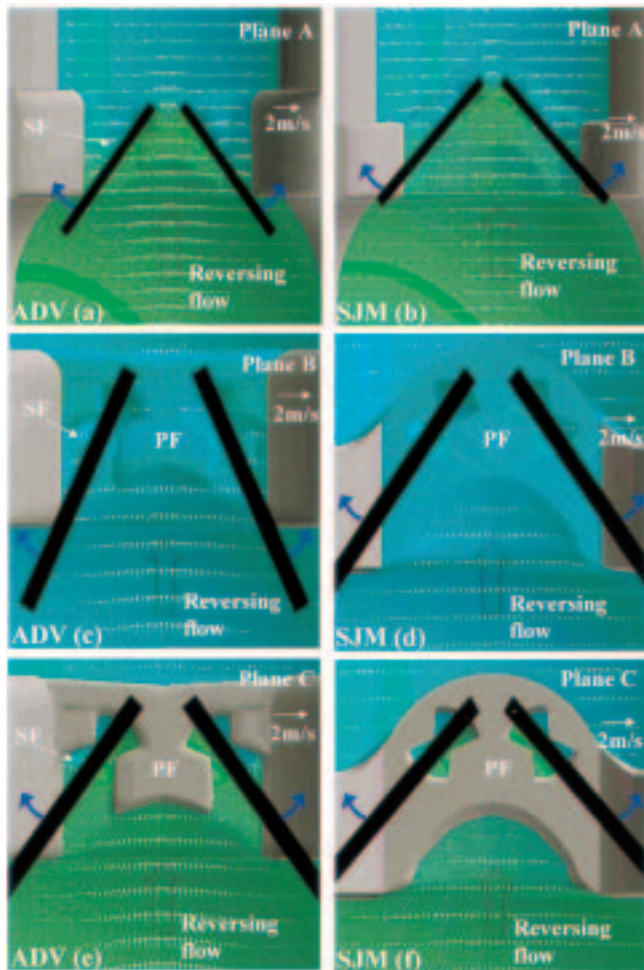


Figure 7: When the leaflets rotate to close, they wipe through the valve pivots. On Plane A, the vena contracta is replaced by reversing flow in the central flow orifice. On Planes B and C, velocity vectors show reversing flow through the channel created by the secondary flat (SF) of the ADV.

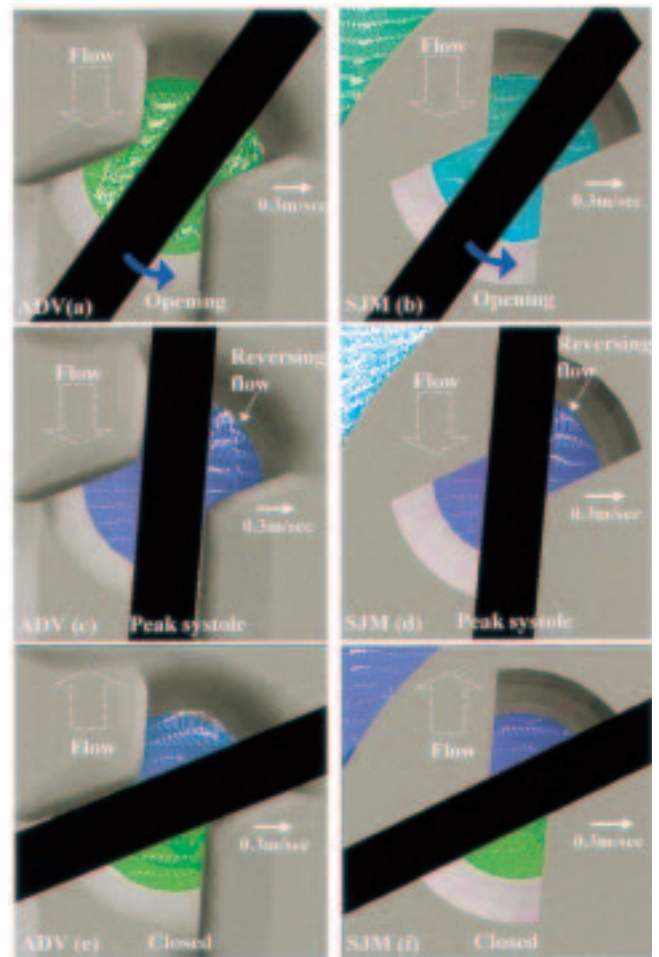


Figure 8: At the two-thirds of the depth of the pivot recess, the simulations on Plane D reveal more dynamic flow activity with larger velocity vectors for the ADV valve than for the SJM valve. At peak systole, reversing flow is observed for both valves. No persistent flow stases are seen inside the pivot recess of either valve.

conditions were taken. The close match in velocity validation between the CFD models and experiment indicated that the models were robust, and the computed flow phenomena in the CFD flow domains replicated the flow phenomena in the pulse duplicator. Because the CFD models were constructed utilizing the dimensions of clinical quality valves, this validation applied also to flow within the pivot, which was part of the CFD model.

The general flow phenomena at the symmetry planes of both valves were similar as expected since both valves are BMHVs. Detailed analysis of the results at the symmetry planes showed a relatively stronger flow jet and large flow boundary separation zones at the central flow orifice of the SJM valve; these flow features were likely due to this valve's smaller central orifice design. The results on these planes also revealed the existence of a waterhammer effect in both valves; this was the first time that the waterhammer effect in BMHVs was demonstrated upon valve closure with a time-dependent 3-D numerical simulation.

At the pivots, flow phenomena closely correlated with the pivot design. In comparison to the SJM valve's single level butterfly pivot, the ADV valve's bi-level butterfly pivot provided a relatively easy passage for fluid within the pivot recess, and promoted more dynamic flow activity within the pivot recess. Because the pivot is the most critical region in a BMHV, the pre-

vention of flow stagnation at the bottom of the recess is desired.

The dynamic flow activity within the ADV valve's pivots was also observed by Saxena and colleagues (5). These authors conducted in-vitro velocity measurements in the pivots of the ADV and SJM valves using laser Doppler velocimetry. The velocity measurements were accomplished at discrete locations on Planes B, C, and D, and the results obtained revealed that the ADV valve had more dynamic flow patterns in its pivots than the SJM valve. This flow feature was also contributed to the ADV valve's bi-level pivot design.

It was noted that in systole, the flow at the bottom of the recess ran counter to the flow through the rest of the valve. This phenomenon has been demonstrated for the first time for BMHVs using CFD simulations, although it had been observed previously in an in-vitro experiment (24). This retrograde flow (seen on Plane D and in the gap) gradually developed before peak systole and diminished near the end of systole. This behavior indicated that gap flow at the bottom of the recess was reversed throughout most of systole. This systolic retrograde gap flow could be attributed to the effect of the vena contracta in the central flow orifice. As the vena contracta had a much higher velocity than flow in the orifice between the leaflet and valve housing during valve opening, its lower flow pressure drew fluid into the central flow orifice through the bottom of the pivot recesses.

In the present study, the ADV valve's CFD model was able to include edge radii in the pivot because it was created directly from a CAD file. By contrast, the SJM valve's CFD model included sharp pivot edges by default because the model was created from measured dimensions (no CAD file was available from the manufacturer). Because different manufacturing methods are used to produce the pivots of these two valves, the ADV pivots have much larger and smoother edge radii than the SJM pivots, as reported previously (24). Compared to the dimensions of its pivot recess, the edge radii in the pivots of the SJM valve are very small. Therefore, inclusion or exclusion of the edge radii in the CFD model of the SJM valve should not affect its basic pivot flow characteristics.

The present study did not use a truly coupled fluid-structure CFD model. Rather, the CFD simulations required the use of known leaflet movements. The position of the leaflet at each millisecond was measured in the pulse duplicator and then provided as a prescribed boundary condition for the simulation. By using this approach, the positions of the leaflet were predetermined as per the experiment and synchronized with the input mass flux waveform. The flow velocities and fluid pressures in the flow domain were then calculated mathematically. In the simulation, the

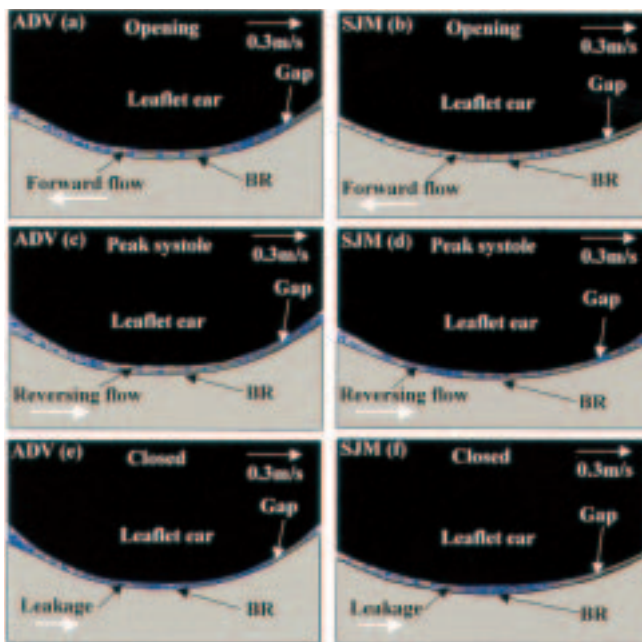


Figure 9: On the plane of the A-A section view (Fig. 1), gap flow occurs between the leaflet ear and the bottom of the recess (BR). At peak systole, retrograde gap flow is seen in both valves. Velocity vectors demonstrate a relatively stronger gap flow in a cardiac cycle for the ADV valve than for the SJM valve.

movement of the leaflet was not driven by the calculated pressure in the flow domain. To overcome this limitation, it is recommended that in future studies, leaflet movement be computed using a truly fluid-structure interaction technology and a pressure-driven approach in a moving cell environment.

The present study also used the nominal design clearances between leaflet ears and housing for the ADV valve and the measured clearances for the clinical quality SJM valve. No assumptions were made about these dimensions. The effect of manufacturing tolerances was not investigated, but for mechanical heart valves the manufacturing tolerances are usually very small and controlled very tightly. Dimensional changes in manufacturing tolerances should not affect the flow characteristics of mechanical valves.

In conclusion, the CFD simulations conducted herein revealed detailed time-dependent flow characteristics within the ADV and SJM valves, with the emphasis at the valve pivots. The simulations demonstrated for the first time the presence of a waterhammer effect upon valve closure and retrograde flow at the bottom of the pivot recesses during valve opening for BMHVs. No persistent flow stases that could indicate thrombogenic flow conditions were observed in the pivot recesses of either valve. The CFD results also confirmed that the ADV valve's bi-level butterfly pivot design provided relatively easy passages for pivot flow washing, and produced more dynamic flow activity within the valve pivots than did the SJM valve's single level butterfly pivot design. However, the benefit of the enhanced pivot flow washing and more dynamic pivot flow activity in the ADV valve design awaits clinical outcomes for confirmation.

### Acknowledgements

The authors thank Dr. Frank Dai for the initial CFD simulation set-up, and Dr. Pushkar Ghosh-Choudhuri for refining the simulation set-up and CFD code modification. They also thank Dave Custer and Susan Ruff for reviewing this manuscript and providing valuable comments and suggestions. The CFD simulation set-up was prepared by Adaptive-Research in California, and funded by Medtronic.

### References

1. Schoen F. Pathologic considerations in replacement heart valves and other cardiovascular prosthetic devices. *Monogr Pathol* 1995;37:194-222
2. Bodnar E. Editorial: The Medtronic Parallel valve and the lessons learned. *J Heart Valve Dis* 1996;5:572-573
3. Gross JM, Shu MCS, Dai FF, Ellis J, Yoganathan AP. A microstructural flow analysis within a bileaflet mechanical heart valve hinge. *J Heart Valve Dis*

- 1996;5:581-590
4. Ellis JT, Healy TM, Fontaine AA, Saxena R, Yoganathan AP. Velocity measurements and flow patterns within the pivot region of a Medtronic Parallel bileaflet mechanical valve with clear housing. *J Heart Valve Dis* 1996;5:591-599
5. Saxena R, Lemmon J, Ellis J, Yoganathan A. An in vitro assessment by means of laser Doppler velocimetry of the Medtronic advantage bileaflet mechanical heart valve hinge flow. *J Thorac Cardiovasc Surg* 2003;126:90-98
6. Christy JRE, Macleod N. The role of stasis in the clotting of blood and milk flows around solid objects. *Cardiovasc Res* 1989;23:949-959
7. Beppu S. Hypercoagulability in the left atrium: Part I: Echocardiography. *J Heart Valve Dis* 1993;2:18-24
8. Yasaka M, Beppu S. Hypercoagulability in the left atrium: Part II: Echocardiography. *J Heart Valve Dis* 1993;2:25-34
9. Keggen LA, Black MM, Lawford PV, Hose DR, Strachan JR. The use of enzyme-activated milk for in vitro simulation of prosthetic valve thrombosis. *J Heart Valve Dis* 1996;5:74-83
10. Yoganathan AP, Corcoran WH, Harrison EC. In vitro velocity measurements in the vicinity of aortic prostheses. *J Biomechanics* 1979;12:135-152
11. Chandran KB, Cabell GN, Khalighi B, Chen CJ. Laser anemometry measurements of pulsatile flow past aortic valve prostheses. *J Biomechanics* 1983;16:865-873
12. Abdullah SA, Shu CS, Hwang NHC. Dynamic performance of heart valve prostheses and testing loop characteristics. *Am Soc Artif Intern Organs Trans* 1983;29:296-300
13. Gross JM, Shermer CD, Hwang NHC. Vortex shedding in bileaflet heart valve prostheses. *Am Soc Artif Intern Organs Trans* 1988;34:845-850
14. Avrahami I, Rosenfeld M, Einav S, Eichler M, Reul H. Can vortices in the flow across mechanical heart valves contribute to cavitation? *Med Biol Eng Comput* 2000;38:93-97
15. Knott E, Reul H, Knoch M, Rau G. In vitro comparison of aortic heart valve prostheses. *J Thorac Cardiovasc Surg* 1988;96:952-961
16. Underwood FN, Mueller TJ. Numerical study of the steady axisymmetric flow through a disk-type prosthetic heart valve in an aortic-shaped chamber. *J Biomech Eng* 1979;101:198-204
17. Greenfield H, Au A. Computer visualization of flow patterns for prosthetic heart valves. *Scand J Thorac Cardiovasc Surg* 1976;10:197-204
18. Dibini G, Pietrabissa R, Fumero R. Computational fluid dynamics of artificial heart valves. *Int J Artif Org* 1991;14:338-342
19. Huang ZJ, Merkle CL, Abdallah S, Tarbell JM.

- Numerical simulation of unsteady laminar flow through a bileaflet tilting disk valve: prediction of vortex shedding. *J Biomechanics* 1994;27:391-402
20. King MJ, Corden J, David T, Fisher J. A three-dimensional, time-dependent analysis of flow through a bileaflet mechanical heart valve: Comparison of experimental and numerical results. *J Biomechanics* 1996;29:609-618
  21. Gao ZB, Hoseun N, Dai FF, Hwang NHC. Pressure and flow fields in the pivot region of bileaflet mechanical heart valves. *J Heart Valve Dis* 1999;8:197-205
  22. Wang JH, Yao H, Lim CJ, Zhao Y, Yeo TJH, Hwang NHC. Computational fluid dynamics study of a protruded hinge bileaflet mechanical heart valve. *J Heart Valve Dis* 2001;10:254-263
  23. Kelly SGD. Computational fluid dynamics insights in the design of mechanical heart valves. *Artif Organs* 2002;26:608-613
  24. Shu MCS, Gross JM, O'Rourke KK, Yoganathan AP. An integrated macro/micro approach to evaluating pivot flow within the Medtronic ADVANTAGE™ bileaflet mechanical heart valve. *J Heart Valve Dis* 2003;12:503-512
  25. Issa RI. Solution of the implicitly discretized fluid flow equations by operator-splitting. *J Comput Physics* 1985;62:40-65